New Journal of Physics
The open–access journal for physics

The lateral photoemission distribution from a defined cluster/substrate system as probed by photoemission electron microscopy

M Munzinger, C Wiemann, M Rohmer, L Guo, M Aeschlimann and M Bauer[1]

Department of Physics, TU Kaiserslautern, Erwin-Schrödingerstr. 46, 67663 Kaiserslautern, Germany
E-mail: mkbauer@physik.uni-kl.de

New Journal of Physics **7** (2005) 68
Received 26 November 2004
Published 22 February 2005
Online at http://www.njp.org/
doi:10.1088/1367-2630/7/1/068

Abstract. We used photoemission electron microscopy (PEEM) to investigate the lateral distribution of the photoemission yield from a defined system of silver clusters supported by a highly oriented pyrolytic graphite (HOPG) substrate. For threshold photoemission using conventional photoemission (PE) and two-photon photoemission (2PPE) we find that distinct, well-separated emitters are responsible for the measured integral photoemission yield. Complementary characterization of the surface using STM shows that the emitter density as probed by PEEM is reduced by about three orders of magnitude in comparison to the actual cluster density. Wavelength and light polarization scans in combination with two-photon-PEEM clearly show that the origin of the 2PPE signal is related to small silver particles. Furthermore, the PEEM differentiates between inhomogeneous and homogeneous broadening effects in the 2PPE signal. This observation allows one to assign the origin of the local photoemission signal to either a distinct single silver particle or a number of coherently coupled silver particles. We conclude that the 2PPE-yield is highly selective with respect to specific properties of the supported silver particles. Our results show that in future experiments, PEEM as a highly local field probe, may be a key tool in the identification of these properties.

[1] Author to whom any correspondence should be addressed.

PII: S1367-2630(05)90385-6

Contents

1. Introduction

Photoelectron spectroscopy (PES) has been widely used in the past to characterize the electronic structure of clusters supported by a substrate [1, 2]. Recently, the technique of two-photon-photoelectron spectroscopy (2PPE) has been applied to study cluster–surface systems and to gain additional information on the excited state distribution [3, 4]. Despite the undisputed and important contribution of PES, e.g., to a better understanding of cluster–substrate interactions, the significance of these results is generally restricted by the lateral integration over a macroscopic area [5, 6]. As a result, it is difficult to avoid inhomogeneous broadening effects in the recorded spectra, even under extremely defined sample conditions. It is also often difficult to exclude definitely a residual uncertainty of these data with respect to the actual origin of the photoemission signal, as a contribution to the PE-signal from the supporting surface is always present. Recently, it has been shown that the use of photoemission electron microscopy (PEEM), capable of a lateral resolution down to 20 nm may overcome this ambiguity [7]. One main aim of this paper is to show that PEEM is in fact a very powerful tool, and can be used to gain information about cluster–substrate systems complementing conventional photoemission experiments.

In the following, we will present our results from a photoemission study of supported clusters at a lateral resolution in the nanometre regime. The chosen system, Ag-clusters on highly oriented pyrolytic graphite (HOPG), has been studied in detail before by means of STM, UPS and 2PPE [2, 4, 5, 8]. This particular system provides reasonable referencing of our measurements to experimental data obtained with well-established techniques in the field. We used photoemission electron microscopy (PEEM) in combination with threshold photoemission, induced by a conventional mercury vapour lamp ($h\nu_{\text{cut-off}} = 4.9$ eV) and the second harmonic of a femtosecond laser-system ($h\nu \approx 3.1$ eV), to probe the local distribution of the electron-yield from a sample of supported silver clusters on HOPG. For the latter case, where the photoemission is the result of a two-photon absorption process, we observe a rather inhomogeneous lateral distribution of the photoemission yield. We find that the dominant signal arises from distinct spots at the sample surface, whereas the intermediate areas barely contribute to the measured overall yield. Complementary STM measurements show, however, that the actual cluster density at the surface is three orders-of-magnitude larger than the structural density visible in the PEEM images. For the 2PPE-yield, from the bright spots, we observe a resonance-like dependence as

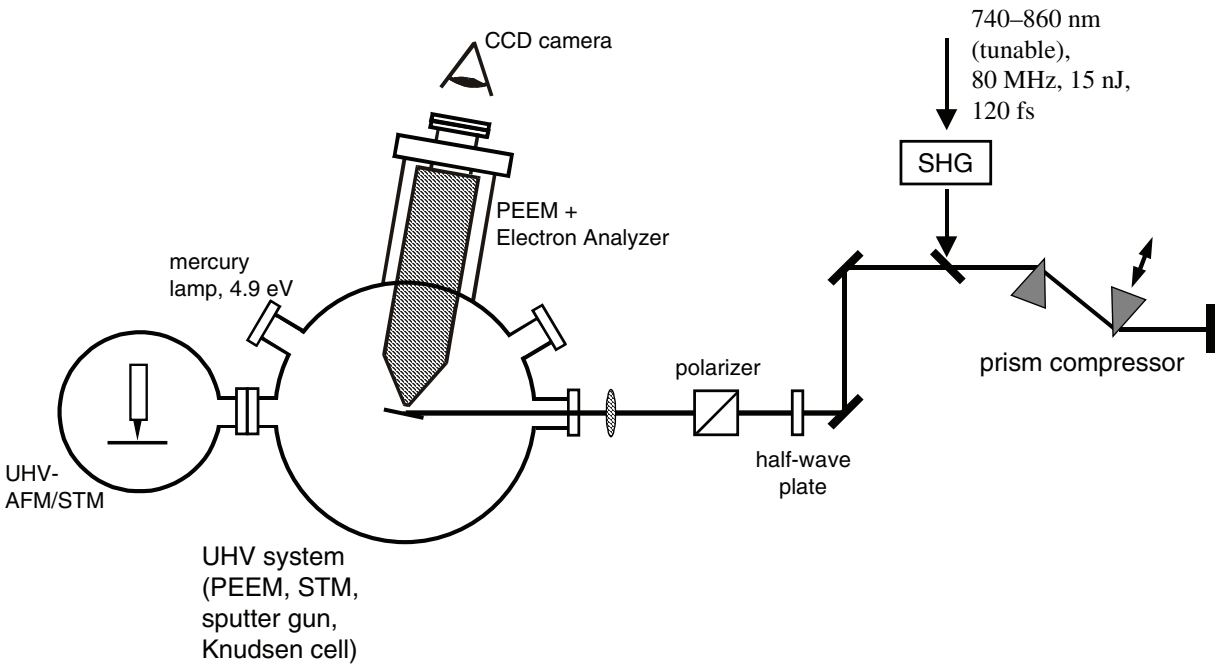

Figure 1. Scheme of the experimental setup.

a function of laser wavelength. We assign this resonance to the excitation of localized plasmon modes, which is characteristic of small silver particles. Furthermore, we find that each spot shows a different wavelength dependence with respect to resonance energy and resonance width. Lateral integration, therefore, leads to an inhomogeneously broadened 2PPE signal. This observation allows one to assign the origin of the localized photoemission spots to either a single emitter or a number of coupled emitters. The discrepancy between STM and PEEM measurements leads us to conclude that nonlinear photoemission does not probe the entire cluster ensemble at the surface, but is highly selective to silver particles with very specific properties.

2. Experimental setup

A schematic view of the experimental setup is shown in figure 1. The commercial PEEM instrument used for our experiments (Focus IS-PEEM) is described in detail in [9]. The microscope is mounted in a μ-metal chamber to shield external stray magnetic fields that would affect the imaging quality of the system with respect to the lateral resolution. The ultimate resolution that can be achieved with the microscope has been specified to 20–40 nm.[2] It is important to note, however, that the possible lateral resolution is not only determined by the specific performance of the PEEM instrument but is also highly dependent on the properties of the sample under investigation. Local electric micro-fields oriented parallel to the surface plane can be induced, e.g., by inhomogeneities in the surface potential, and can strongly affect the electron trajectories on their way to the microscope. In the presence of such fields, the

[2] The lateral resolution of the used PEEM system has been determined in threshold photoemission from the work-function contrast at a step ($\Delta I_{16-84\%}$).

size of an object determined from the PEEM image can exceed the size of the actual object at the surface many times over [10, 11]. Two different light sources have been used to record PEEM images: a conventional mercury vapour UV source (energy cut-off at 4.9 eV) and a Ti : sapphire laser system. Using the mercury vapour lamp, the lateral distribution of near-threshold photoemission is imaged by the PEEM. In the case of the pulsed femtosecond laser system, the high peak intensities of the output create nonlinear photoemission by means of multi-photon photoabsorption. For the present experiments the fundamental output of a tunable femtosecond Ti : sapphire laser system (80 MHz, 120 fs, 750–850 nm) is frequency-doubled in a 0.2 mm-thick beta barium borate (BBO) crystal to produce UV light at $h\nu = 2.9$–3.3 eV. These ultrashort UV pulses are focused onto the sample so that intensities high enough to induce two-photon photoemission are achieved. Within such a nonlinear photoemission process, not only the ground-state electronic distribution is probed but also electronic excitations located between the Fermi-edge and the vacuum level.[3] For some of the experiments the orientation of the electric field vector of the laser-light has been rotated (from p to s polarization) by the use of a zero-order half-wave plate in combination with a Glan–Thompson polarizer. Along with the PEEM system, a commercial UHV-STM (Park Scientific Instruments, VP) is attached to the chamber and makes characterization of the surface topography possible; sample transfer between both systems is performed *in situ*.

For sample preparation, the chamber is equipped with a commercial sputter gun, an e-beam heating stage, a Knudsen cell-type evaporation source and a quartz thickness monitor.

3. Sample preparation

The preparation of the supported clusters follows the procedure introduced by Hövel and co-workers, which has been described in detail in [13]. On a tape-cleaved and vacuum-annealed (600 °C, 1 h) HOPG surface, atomic defects are created by argon sputtering for 20 seconds at 1 keV kinetic energy. Subsequent oxidation in air at a temperature of 530 °C for 8 min results in the formation of small etch pits in the topmost layer of the graphite. After a second vacuum annealing at 600 °C (1 h), nominally three MLs of silver were evaporated onto the surface ($T = 300$ K, 0.085 nm min^{-1}). Condensation of the silver in the preformed pits results in the creation of silver clusters at a rather narrow size distribution, with $\Delta h/h$ of the order of 0.2, where h is the measured height of the clusters [13, 15]. Figure 2 shows a STM scan of our surface over an area of 250×250 nm^2 of the HOPG after silver deposition, showing the typical topographic features of these systems as described in STM studies before [4, 13]. In agreement with these publications, we are able to differentiate two different types of condensed cluster species. At a density of about 2400 μm^{-2}, single separated clusters are formed as a result of condensation in the artificially created small pits. Cluster decoration along edges, at a significant higher local density, is also observable, as seen at the border of large pits in the bottom right corner of figure 2. Note that the appearance of these large pits next to the small pits is not a substrate intrinsic property, but results from the specific preparation process of the HOPG substrate prior to evaporation [14]. For the separated clusters, we observe a certain tendency to appear in pairs (figure 2). Although this behaviour has not been mentioned before, it agrees with observations by Hahn and Kang who reported the frequent creation of pit pairs in the graphite substrate as a result of the sputtering process [14]. An estimate of the cluster diameter can be given from

[3] For an overview on 2PEE and its application to different systems, see e.g. [12].

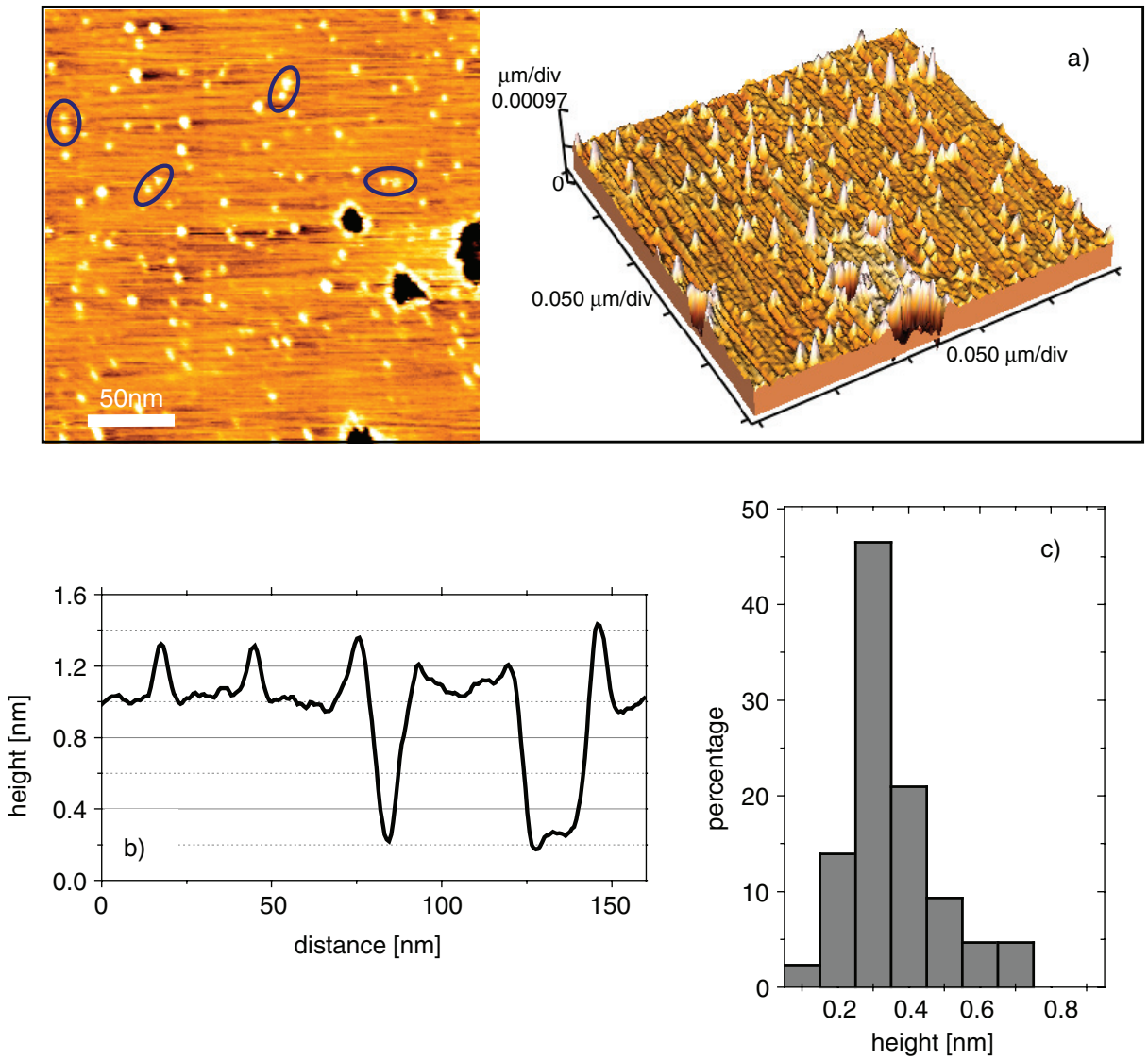

Figure 2. Topography of the prepared HOPG-substrate after deposition of 3 MLs of silver (250 × 250 nm; 0.3 V bias; 230 pA current); a homogeneous distribution of single, separated clusters are observed, which shows a tendency to appear in pairs (examples are marked); in addition, we find high-density step decoration at large-size holes; note that the depth of the large holes is 2 ML (see height profile (b) along the white line indicated in (a)) in agreement with [14]; the measured height distribution of the separated clusters is shown in (c).

its lateral extension as visible in the STM image. We observe a typical size of 7 nm with only small variations from cluster to cluster (maximum ±1 nm). Note, however, that for objects of this size, the convolution of the STM-signal with the tip-shape can lead to an inflation of the lateral cluster extension [5], so that this value is only an upper limit of the actual cluster diameter. Alternatively, the mean size can be estimated from the deposited quantity of silver (3 ML) and the measured cluster density of (2400 μm^{-2}). For a sticking coefficient of silver at 300 K of

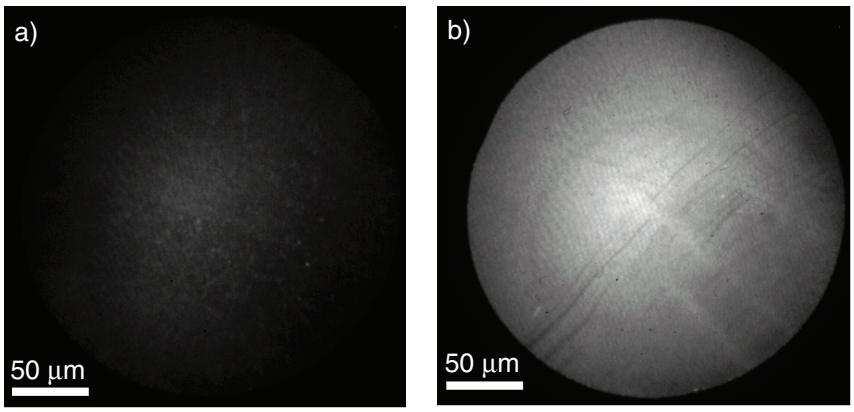

Figure 3. PEEM images of the pure HOPG substrate (a) and after the evaporation of 3 ML of silver (b) using a mercury vapour lamp (field of view: 250 μm); note that the images do not show the same area at the surface; for (b) a strong enhancement in the photoemission yield in comparison to the HOPG is obvious. The origin of the visible structures is described in the text.

about 0.5 [5], we calculate a diameter of 6 nm which is very close to the value obtained directly from the STM image. The measured height of the clusters may also be used to determine the actual cluster diameter, as the shape of the clusters is only slightly distorted by the interaction with the HOPG substrate. A constant height to diameter ratio of 0.7 has been observed for the silver clusters independent of cluster size [13]. In the present case, the average height is about 0.3 nm (see figures 2(b) and (c)). This value is obviously considerably smaller than the estimations for the cluster diameter given above, even if we consider that the clusters immerse into the pits with a depth of 0.35 nm. The reason for this very significant deviation is not yet clear, but may be attributed to distortions within the STM scan, such as a partial removal of silver from the clusters during the scan (even though careful scanning parameters have been chosen for imaging). For the purposes of this paper, accurate knowledge of the mean cluster size is unnecessary and we will henceforth refer only to the upper limit (7 nm) of the cluster diameter.

Besides the characterization of the topography of the deposited clusters, the STM tip was also used to remove the clusters from their pits, thereby creating completely uncovered HOPG reference areas for the PEEM measurements. At sufficiently high tunnelling currents and voltages, such a procedure can be highly efficient. In the present case, typically a current of 1.5 nA at a voltage of 3 V has been used. The corresponding areas could be identified in the PEEM images as areas showing strongly reduced photoemission yield characteristic of an uncovered HOPG substrate (figure 8).

4. PEEM results and discussion

Figure 3 shows conventional PEEM images for the pure HOPG surface (figure 3(a)), and after deposition of silver (figure 3(b)), obtained with the mercury vapour lamp. The field of view in both cases is about 250 μm in diameter. The enhancement of the photoemission signal after evaporation of silver is clearly visible in comparison with the pure HOPG substrate. In figure 3(b) black, line-shaped features extend from the bottom left to the top right of the image and most

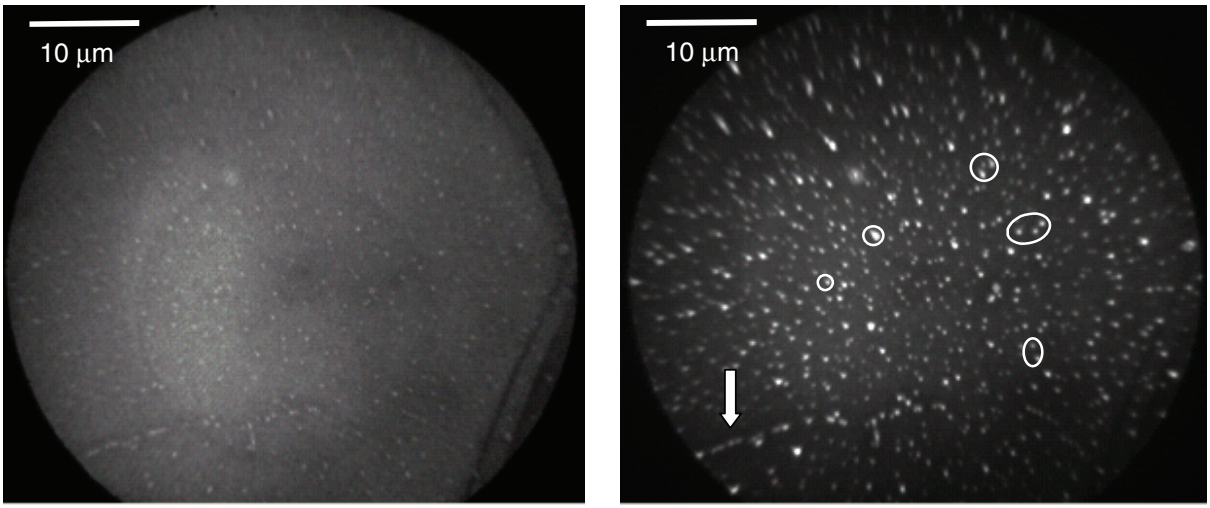

Figure 4. PEEM images of the HOPG substrate after silver deposition, at a field of view of 50 μm, recorded using the mercury lamp ($h\nu = 4.9$ eV) (a) and the SHG of the laser output ($h\nu = 3.1$ eV) (b); white circles in (b) indicate examples of bright spots visible in the 2PPE image, but not present under irradiation using the mercury vapour lamp (1PPE).

likely arise from large step defects in the substrate. The intensity reduction observed for this feature is not related to a reduced silver coverage in this area, but rather to shadowing effects as the UV light is incident from the right at an angle of 25° with respect to the surface plane. Otherwise, on this scale, the photoemission yield seems to be homogeneously distributed.

In figure 4 the overall field of view of the PEEM images has been reduced by a factor of 5 to approximately 50 μm. Both images show the identical area of the silver covered HOPG recorded using the mercury vapour lamp (figure 4(a)) and the frequency doubled output (3.1 eV) of the laser system (figure 4(b)), respectively. At this magnification, a clear spot-like structure in the photoemission yield is visible from the surface for both excitation processes (1PPE and 2PPE). Whereas for 1PPE, the contrast of these spots as compared to the background is rather weak, and is much more pronounced in the case of the nonlinear (2PPE) imaging (figure 4(b)). Furthermore, only some of the spots visible in the 2PPE image are visible in the 1PPE image. This effect is not only due to the reduced contrast in the 1PPE process, but is related to the excitation process itself (1PPE versus 2PPE), as even some of the brightest and largest spots visible in the 2PPE image (figure 4(b)) have completely disappeared in the 1PPE image (figure 4(a)). On the other hand, some spots that appear rather weak in the 2PPE image are still present in the 1PPE image. Next to the homogeneous distribution of bright spots, aligned spots are also visible, typically going along with an intensity depletion in the close surrounding distance of the order of 1 μm. One distinct example (marked with an arrow) can be found at the bottom left corner of figure 4. The appearance of these features may be indicative of the decoration of the substrate steps by the silver; however, the origin of the depletion zone is not yet clear. The diameter of the spots visible in the PEEM images is of the order of 200–300 nm. However, the measured size of a single spot differs depending on the chosen excitation source (mercury lamp or laser), where the dependence is not systematic: we find spots that appear larger in the 1PPE image than in

the 2PPE image and vice versa. This observation indicates that the PEEM image, does not give information about the actual topography of the emitters, as the topography should not depend on the excitation wavelength. Possible static mechanisms that can account for such distortions have already been discussed in section 2. The dependence of the visible emitter size on the excitation wavelength indicates that dynamical effects related to the details of the photoemission process may need to be considered in this connection.

The most obvious question that arises from a comparison of the STM data in relation to the surface topography (see section 3) and the PEEM images is the following: to what extent can the photoemission signal be related to the cluster distribution at the HOPG surface? The evident discrepancy between PEEM and STM is the observed structure density; we find approximately the same spot number within an area of about $8 \times 8\,\mu\text{m}^2$ for the PEEM image (figure 4) in comparison to an area of $0.25 \times 0.25\,\mu\text{m}^2$ for the STM scans (figure 2). Note that the visible size of a bright PEEM spot in figure 4 (about 200–300 nm) covers approximately the scan area shown in figure 2(a). This means that the structure density visible by the two microscopic techniques deviates by about three orders of magnitude. Consequently, it is not *a priori* clear that the photoemission signal arises from silver particles as visible in the STM. In the following we will see, however, that the 2PPE from these bright spots shows properties characteristic of small silver particles.

For these investigations, we make use of the degrees of freedom offered by the chosen laser system, namely the wavelength and the orientation of the polarization vector of the laser field. We will show that such an approach enables us to specify, to a certain extent, the origin of the PE-yield. We find that the 2PPE from the bright spots in the PEEM images is mediated by the coupling of the laser light to localized collective excitations, which are characteristic of small silver particles. In addition, we can show that the details of the 2PPE process are different for each spot. In the lateral integrating photoemission experiment, this gives rise to inhomogeneous broadening effects. By contrast, PEEM is capable of separating this inhomogeneous contribution from the 2PPE signal and allows us to make further statements about the nature of these local emitters.

4.1. Spectroscopy: wavelength scans

The femtosecond laser system enables a wavelength tuning between 750 and 850 nm corresponding to 375–425 nm (3.3–2.9 eV) for the second-harmonic generation (SHG). The bandwidth of the frequency-doubled laser-pulses is approximately 10 meV. For the PEEM images, we find a strong dependence of contrast and structure distribution as a function of incident wavelength. Figure 5 shows the same area of the sample recorded at a wavelength of 375 nm (figure 5(a)) and 415 nm (figure 5(b)), respectively. For the longer wavelength, the contrast between bright spots and quasi-homogeneous background is significantly reduced. In addition, the relative intensity ratio between separate features is changed. Distinct examples are marked in the image by arrows and the corresponding details are described in the figure caption. For a quantitative discussion of these changes, the raw data obtained from the wavelength scan must be corrected with respect to changes in the laser pulse intensity as a function of wavelength.[4] As a reference level, required for the correction procedure, we used the background 2PPE-intensity in the PEEM images interstitial to the bright spots. We then chose a defined threshold level

[4] The critical parameter in this connection is not the average laser power, which can be kept constant within a wavelength scan, but rather the temporal width of the laser pulses.

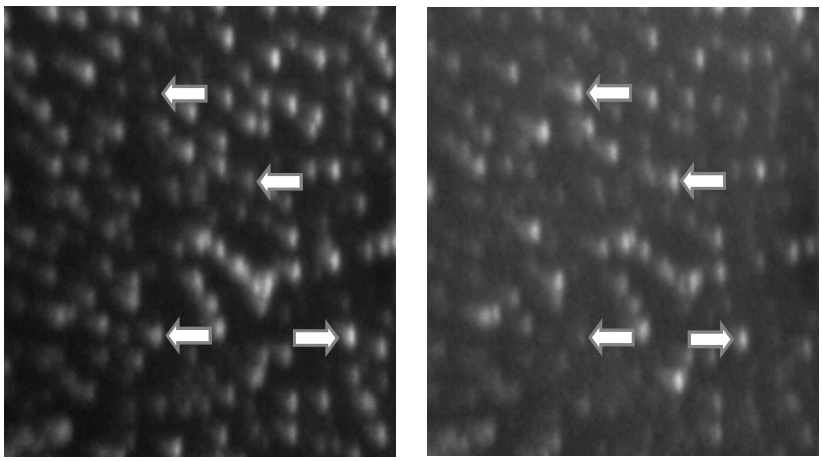

Figure 5. PEEM images recorded at a laser wavelength of 375 nm (a) and 415 nm (b); the size of the displayed area is about $8 \times 8\ \mu m^2$. The slight ellipticity visible for all spots results from some amount of astigmatism of the microscope at the used settings. Note that the laser intensity and exposure time differ for both images; therefore, the absolute value of the grey scale cannot be compared. The change in the relative contrast of the bright dots with respect to the homogeneous background is obvious; details in the visible-spot structure change; in relation to each other, most spots become dimmer, and a few become brighter with increasing wavelength; examples are marked by grey arrows.

within the grey scale of the corrected images to create a black-and-white representation of the original images, where 2PPE intensities above the threshold level appear black. A black dot in the corrected images corresponds, therefore, to a bright spot in the original PEEM images. The size of the black dot is proportional to the 2PPE-yield from this spot. In this way, the measure for the normalized overall 2PPE intensity from a chosen field is given by the size of the overall black area contained. By focusing onto a specific feature in the PEEM image we quantified the wavelength dependence of a single bright spot.

Figure 6(a) shows a series of PEEM images as functions of wavelength edited according to the procedure described above. The wavelength dependence already discussed for figure 5 is again clearly visible. The overall tendency towards smaller black dots with increasing wavelength corresponds to a reduced 2PPE intensity from the bright PEEM spots, and reflects the reduction in contrast in comparison with the background. The structural changes as a function of wavelength are obvious. A quantitative analysis with respect to the overall dependence can be performed in two ways: the overall integral over the black area of an image as a function of photon energy can be calculated, or the number of black dots visible in the images can be counted. The results obtained from these two analysis modi are displayed in figures 6(b) and (c) as a function of photon energy (note that the y-axis has been inverted for better comparison with figure 6(d)). For both cases, we observe qualitatively the same wavelength dependence. The number of visible dots (b) and the integrated 2PPE intensity (c), respectively, increases monotonically but not linearly with increasing photon energy and seems to level off at about 3.2 eV. Slight deviations between the two representations are observable in the low-energy tail of the trace, where the dot-counting

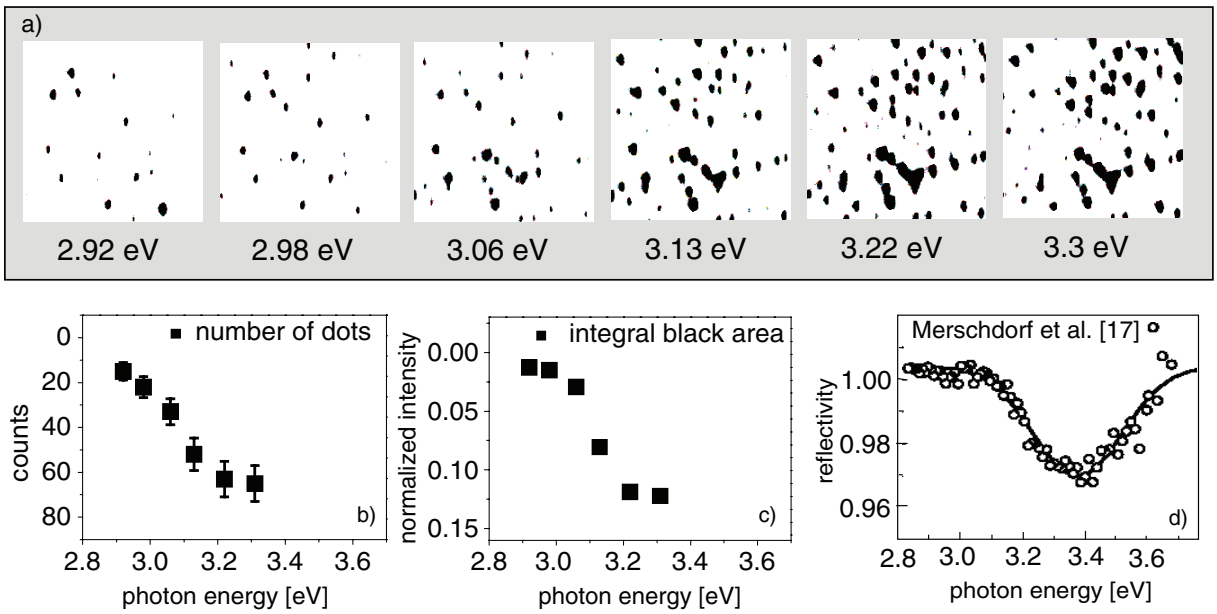

Figure 6. Quantification of PEEM images obtained from a wavelength scan; (a) photon energy dependence after normalization of the PEEM data as described in the text; (b) number of dots/image in (a) as a function of excitation energy; (c) integral black area of each image in (a) as a function of excitation energy; (d) reflectivity data for silver clusters/HOPG as published by Merschdorf *et al* [15]; *y*-axes of (a) and (b) have been inverted for easier comparison with (c); agreement between our PEEM data and the integral 2PPE data in the overlapping wavelength regime is remarkable.

procedure gives rise to larger relative values in comparison to the intensity integration procedure. This means that spots that are most pronounced at low photon energies show on average a reduced 2PPE-yield as opposed to spots that are dominating the visible structure close to the intensity plateau. Due to the restricted wavelength regime of the laser system, measurements at higher photon energies were not possible.

A comparison of our data with reflectivity data obtained from silver clusters deposited on graphite under equivalent conditions is intriguing (figure 6(d)) [15]. Within the wavelength regime accessible in our experiment, the highly local results from the PEEM measurements are in almost perfect agreement with these lateral integrating reflectivity data and integral 2PPE data [15]. It is therefore rather reasonable that, within the latter study, an equivalent, highly structured lateral photoemission distribution has been probed. This distribution becomes, however, visible only within a PEEM study as presented here. The possible origin of the observed increase in the 2PPE-yield and the intensity drop of the reflectivity in the photon energy range between 3 and 4 eV have also been discussed in detail [15]. Such a resonance like behaviour is characteristic for the excitation of localized particle plasmons in small silver nanoparticles and clusters [16]. For free and spherical silver particles with a diameter <10 nm, the resonance energy is located at about 3.5 eV. Interaction of the particle with a surrounding medium typically results in a red-shift of this resonance. On the other hand, a blue-shift of the resonance can be observed with decreasing cluster size due to a reduction in the screening efficiency of the

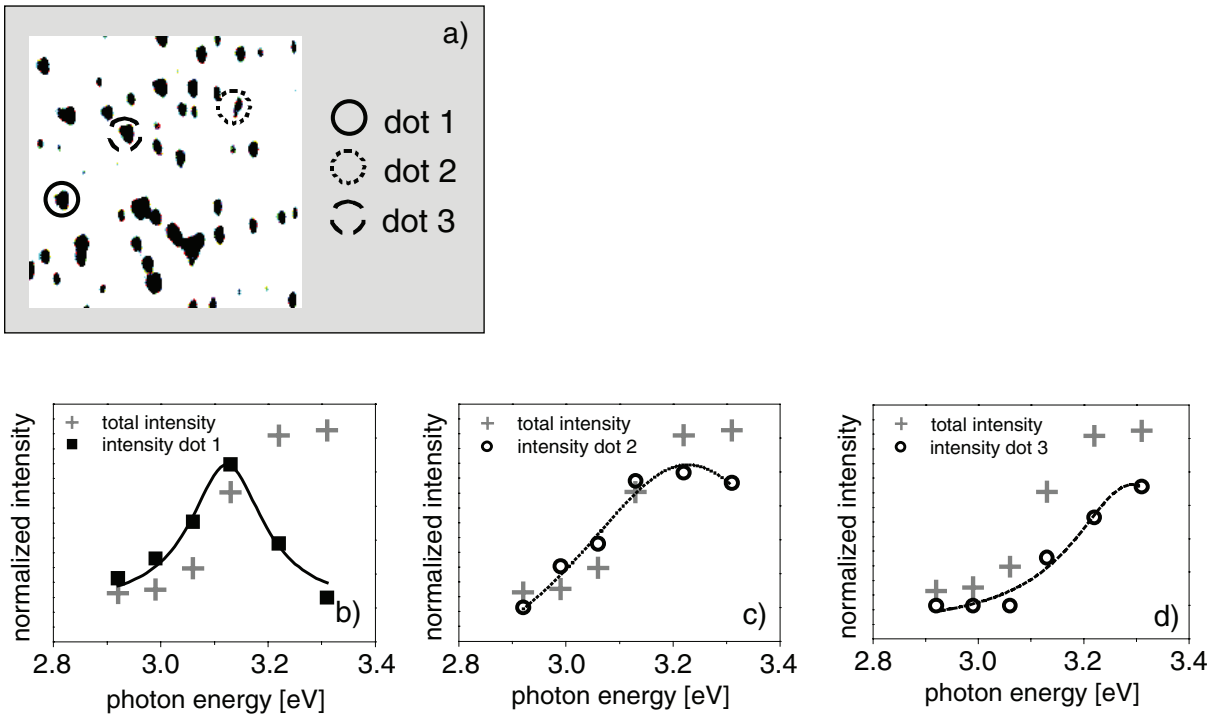

Figure 7. Local spectroscopy of three single dots as marked by circles in figure 7(a); (b)–(d) dot intensity as a function of excitation energy; lines are Lorentzian fits to the experimental data; for dot 1 a resonance like behaviour is noticeable; the clearly differing wavelength dependence of the three dots show that the integral dependence (indicated by the grey crosses) is strongly inhomogeneously broadened.

localized 4d-electrons in silver [17, 18]. Furthermore, deformation of the clusters, due to the interaction with the substrate, lifts the degeneracy of the three plasmon modes corresponding to excitation along the three main axes of the spheroid. On comparing with [15], we conclude that in the present experiment, the coupling of the lasers light to localized plasmon modes of supported small silver particles gives rise to the observed resonance-like behaviour in the 2PPE-yield. The new and important conclusion that can be drawn from the PEEM data is that not all silver particles present at the surface contribute to the signal in the same way. Instead, the 2PPE process resulting from the coupling to such plasmon modes seems to be highly selective to specific areas of the surface.

A closer look at the wavelength dependence of a single PEEM spot, can give further information on the nature of the emitter. A detailed single spot analysis has been performed for three spots of the image area marked with circles in figure 7(a). The corresponding wavelength dependence is shown in figures 7(b)–(d) in comparison to the integral wavelength dependence of the entire area (grey crosses). The maximum intensities from the three dots have been normalized for better comparison and a Lorenz-fit has been added to each trace. For dot 1 it is obvious that the 2PPE-yield shows a resonance-like behaviour with a maximum intensity located at an energy of about 3.1 eV, well below the expected resonance energy of about 3.4 eV for the integral dependence. Due to the restricted wavelength regime accessible with the laser system, a complete resonance curve could not be scanned for dots 2 and 3. The general trend clearly

points to a resonance-like behaviour shifted in energy into the blue in comparison with dot 1. Note that the three features were selected rather arbitrarily from the image area above[5] and a qualitatively similar behaviour is found for most of the other features in figure 7(a), as well. Obvious deviations from a resonance behaviour are typically found in cases where two dots are very close together and a clear distinction between them is not possible.

The linear response of the plasmon excitation is proportional to the square root of the second order 2PPE-yield signal. The FWHM of a Lorentz fit to this trace gives an estimate of the lifetime of the plasmon. For dot 1, where the resonance maximum is clearly crossed in the wavelength scan, we obtain a value of about 310 meV from such a fit. This is twice the value for a free silver cluster of about 1 nm diameter [19] and almost identical to the linewidth measured in a local STM experiment for individual clusters of 2 nm diameter deposited on Al_2O_3 [18]. It corresponds to a lifetime of the plasmon excitation of about 2 fs.

These PEEM results clearly show that the resonance peak obtained from integral measurements (reflectivity and photoemission) is significantly broadened due to inhomogeneities in the properties of the probed silver particles. As has been shown before in local photon emission spectroscopy using STM [18], the local probing of distinct features, in this case by PEEM, allows one to deconvolute these inhomogeneous contributions in an efficient manner. Furthermore, the fact that different photoemitters are distinguishable by their specific resonance properties is a very strong indication that the photoemission source is either a single silver particle or a number of at least coherently coupled emitters. Potential candidates for the latter case are, e.g., the cluster ensembles decorating the edges of large holes' as described in connection with the STM image (figure 2). If a number of completely independent emitters are responsible for a distinct spot, we would expect the same inhomogeneously broadened resonance shape as observable in the integral 2PPE measurements. On the other hand, if the origin of a bright PEEM spot is a single silver particle, the observed differences in the resonance shift and broadening could be assigned either to differences in the coupling of the particles to the graphite substrate or differences in the particle shape and size [16]. Size effects, in particular, have been previously identified to be a possible source of an inhomogeneous broadening of the plasmon resonance. For individual silver clusters on Al_2O_3/NiAl (110) for example, a blue-shift of the order of several 100 meV with decreasing cluster diameter was observed in the sub-10 nm regime [18]. This shift is accompanied by a homogeneous line-broadening due to enhanced surface scattering rate of the plasmon with decreasing cluster size. In this context, the visible inhomogeneities of our local PEEM data may be attributed to the inhomogeneous size distribution of the silver clusters. However, we have to admit that the limited wavelength regime in this study does not yet allow conclusive statements about the correlation between plasmon energy and plasmon width.

4.2. Light polarization scans

The dependence of the measured photoemission yield on the orientation of the electric field vector of the exciting laser light with respect to the surface normal, can give further information on the origin of the bright spots visible in the PEEM images. For 2PPE from plane surfaces, typically a $\cos^4(\vartheta)$ dependence on the polarization angle ϑ is reported, which is indicative of an exclusive dipole-resonance excitation perpendicular to the surface [20]–[22]. We find exactly this behaviour for the pure HOPG surface in agreement with [23]. For inhomogeneous surfaces, a polarization dependence strongly deviating from this behaviour has been reported [20, 21].

[5] The choice was only adjusted to show three examples with obviously different resonance energies.

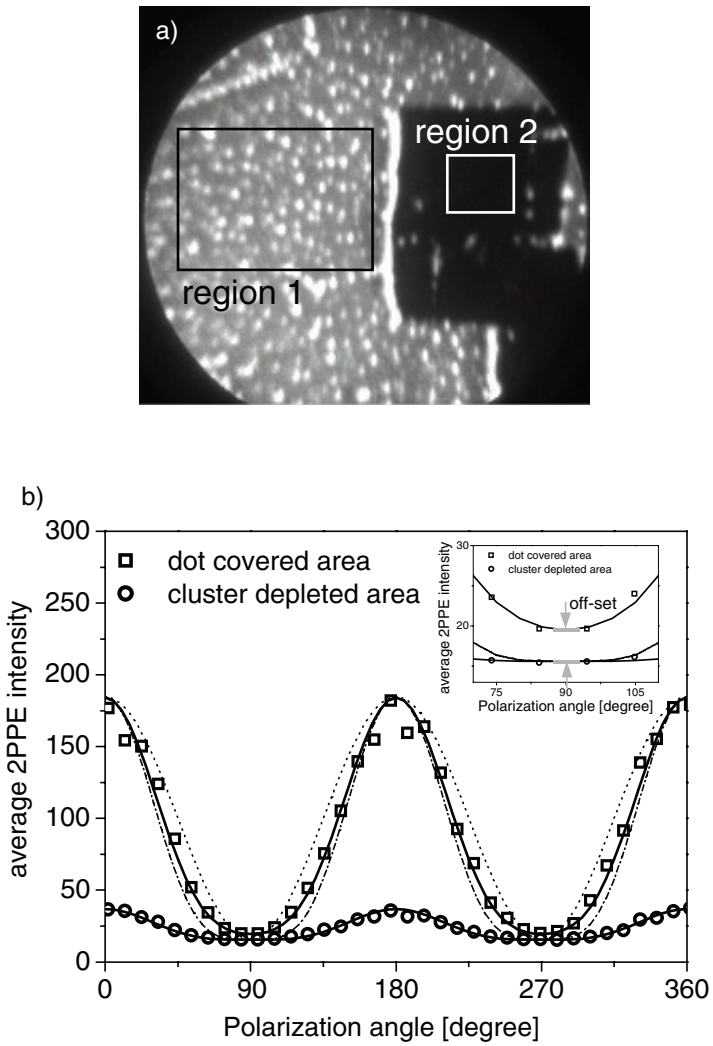

Figure 8. Dependence of the 2PPE-yield from the polarization vector of the exciting laser light. (a) PEEM-image of the probed area; (b) polarization dependence as obtained by averaging over the two areas indicated in (a); 90° corresponds to excitation with s-polarized light (polarization vector has no component parallel to the surface normal); open squares show the results for the silver-covered area (region 1, black square in (a)), open circles show the results for the area depleted using the STM (region 2, white square in (a)); the lines are calculated traces in the case of a $\cos^2$ dependence (· · · · · ·), a $\cos^4$ dependence (–·–·–) and a dependence as discussed in the text and adjusted to the data from region 1; the inset shows the polarization dependence of the traces close to the 90° polarization angle to highlight the intensity offset of region 1 in comparison to region 2.

The lack of information on the structural shape of the features probed in these experiments does not allow for a meaningful model of the actual polarization dependence.

Results from 2PPE-yield measurements as a function of the polarization angle of the incident laser light for the silver-covered HOPG surface are summarized in figure 8. The corresponding

PEEM image is shown in figure 8(a). Figure 8(b) shows the dependence of the 2PPE-yield as a function of polarization angle. A polarization angle of 0° corresponds here to p-polarized light, i.e., the electric field vector contains components perpendicular and parallel to the surface. For the 90° polarization angle (s-polarized) the electric field vector contains no component perpendicular to the surface. The two experimental traces in figure 8(b) have been extracted by integration and averaging over the marked areas indicated by the rectangles in figure 8(a), as a function of light polarization angle. The position of the black-lined rectangle (region 1) has been chosen to cover a field where a rather homogeneous distribution of bright spots is found. The white border rectangle (region 2) is, however, located in a field that has been scanned by the STM in a destructive way, as described above in section 3, prior to the PEEM measurements. The dramatic reduction in the 2PPE-yield from this area shows that the silver has been completely removed by the STM tip and that the pure HOPG surface is probed by the PEEM. We find distinct differences in the polarization dependence in the 2PPE-yield from these two areas. The signal from the pure HOPG field (○, figure 8(b)) shows a dependence very close to a $\cos^4(\vartheta)$ behaviour, as expected for a plane surface. The same behaviour was observed for the HOPG surface prior to the evaporation of silver. The 2PPE-yield from the silver covered area (□, figure 8(b)) shows a dependence significantly deviating from this behaviour in two aspects: (1) the overall shape of the trace no longer follows a $\cos^4(\vartheta)$ law (for comparison, such a dependence is indicated by the dash-dotted line in figure 8(b)). In particular, the broad intensity plateau located around an angle corresponding to s-polarized light (90° and 270°) and characteristic of a $\cos^4(\vartheta)$ dependence is significantly narrowed; and (2) for s-polarized light, the intensity level from the silver-covered area is increased in comparison to the reference signal from the pure HOPG area (inset, figure 8(b)).

Let us consider the expected polarization dependence of the 2PPE-yield for a silver particle which is distorted in the axis perpendicular to the surface (in the following labelled as z-axis) due to e.g. the interaction with a surface or due to a modification in the length of this axis with respect to the perpendicular plane. The coupling of the laser field to the plasmon resonances in the silver particle results in a field enhancement of the internal electric field which is responsible for a photoemission yield detected by the PEEM. The projection of the electric field vector onto the three main axes of the silver spheroid allows us to consider conveniently the enhancement due to the plasmon excitation

$$\vec{E}^{tot}_{\text{int}} = E^x \cdot a_x \cdot \hat{e}_x + E^y \cdot a_y \cdot \hat{e}_y + E^z \cdot a_z \cdot \hat{e}_z.$$

Here, $\vec{E}^{tot}_{\text{int}}$ corresponds to the total internal field inside the particle. E^i $(i = x, y, z)$ are the projections of the external fields onto the respective main axes and a_i are the corresponding field enhancement factors due to the coupling to the localized plasmon modes. Due to the assumed symmetry properties of the particle, we have to set $a_x = a_y$, whereas the particle distortion along the z-axis leads in general to $a_x \neq a_z$. The field-intensity I^{tot}_{int} responsible for the photoemission is proportional to $(\vec{E}^{tot}_{\text{int}})^2$ and given by

$$I^{tot}_{\text{int}} = (E^x \cdot a_x)^2 + (E^y \cdot a_y)^2 + (E^z \cdot a_z)^2.$$

The 2PPE-yield shows a quadratic dependence on the field intensity and is therefore proportional to$(I^{tot}_{\text{int}})^2$. When $a_x,\ a_y \ll a_z$, under far off-resonant conditions with respect to the plasmon modes oriented parallel to the surface and resonant conditions for perpendicular excitation, the well-known $\cos^4(\vartheta)$ dependence occurs.

In order to fit the measured polarization dependence of this model, the only relevant parameter that can be adjusted is the ratio $a_x/a_z(=a_x/a_z)$. The result of such a fit is shown as a solid line in figure 8(b). The agreement between experiment and calculation is good, particularly, if one considers that the trace has to reproduce not only one, but two distinct deviations from the pure $\cos^4(\vartheta)$ listed in figure 8(b). For the present case we find for the relevant fitting parameter a^x/a^z, a value of approximately 1/3. The observed modified angular dependence and the finite 2PPE-yield at 90 and 270° results from the additional dipole excitation in the x- and y-directions due to the coupling of the light to the corresponding plasmon modes.

In addition to the wavelength results, the characteristics of this polarization dependence and the good agreement with our model is further proof that the observed bright PEEM spots are related to nonlinear photoemission from small and rather defined silver particles. We would like to mention that, for the polarization scans, our (local) results deviate from the (integral) observations by Pfeiffer and co-workers [23], who find for the silver clusters a behaviour similiar to a $\cos^4(\vartheta)$ dependence. Several factors, however, can determine the details of the measured traces, such as the localization of the excitation wavelength with respect to the resonance energies of the involved plasmon modes. Another important difference may be the mean diameter of the deposited silver clusters [23].

5. Outlook

Our PEEM results show that the interpretation of lateral integrating photoemission data of cluster–surface systems—particularly in the case of nonlinear photoemission—is not necessarily straightforward. The enormous discrepancy between signal densities obtained with PEEM and that obtained by STM, from a rather defined cluster–surface system, indicates that 2PPE is selectively addressing specific areas of the surface. The wavelength and polarization scans performed show that the measured signal is related to distinct properties of small silver particles. However, from our experiments and laterally integrating 2PPE experiments published before [4, 8, 15, 23], no conclusions on the specific particle property can be made that governs the 2PPE-yield. Potential reasons for the high selectivity of 2PPE may be differences in the particle size, shape, or the coupling to the substrate. In addition, the interaction of closely lying particles, which can affect plasmon characteristics and the local field distribution going along with this excitation [24], may have to be taken into account. In the present case, the tendency for cluster pairs to appear as well as the high-density decoration of the borders by of large-size holes (STM scan in figure 2(a) may give rise to these effects. Finally, it is important to keep in mind that the nonlinearity of the 2PPE process can drastically amplify inhomogeneities of the cluster–substrate system. This may be one of the reasons why the corresponding 1PPE image recorded with the Hg-lamp appears more homogeneous.

The combination of PEEM and STM presented in this paper is the first attempt to correlate results from a cluster–substrate system obtained with these two microscopy techniques. Our results show that a definite assignment of a local photoemission feature to a specific particle/cluster property requires further improved local correlation between PEEM and STM. The goal is to probe identical areas in a complementary way by PEEM and STM. The potential of STM to set clearly identifiable local markers at the surface in a PEEM image, as shown above, is a first and important step in this direction.

Overall, we believe that PEEM can be a highly efficient experimental tool to close the gap between macroscopic integration PES and highly localized scanning probe microscopy of cluster–surface systems.

6. Summary

We have shown that the lateral distribution of the nonlinear photoemission yield from a defined system of supported clusters can be rather inhomogeneous. The huge discrepancy between cluster density as determined by STM and the structure density as visible in the photoemission image caused us to consider, in more detail, the origin of the actual photoemission signal. In the present work, we were able to show that the 2PPE arises from a coupling of the exciting laser light to either single, small silver particles or a number of coupled silver particles, e.g. condensed at high density at the border of large holes in the HOPG substrate. Furthermore, we could show that, for the system under investigation, the integral 2PPE data are significantly broadened due to inhomogeneities in the emitter properties. A local resolving technique such as PEEM allows for focus on the homogeneous contribution to the signal broadening. We propose that in future, locally highly correlated photoemission and STM experiments will be possible and will allow a significantly improved interpretation of photoemission from cluster–surface systems.

Acknowledgments

Special thanks to M Cinchetti for helpful discussions and critical comments on various aspects of this manuscript. This work was supported by the Deutsche Forschungsgemeinschaft through SPP 1153.

References

[1] Wertheim G K, DiCenzo S B and Youngquist S E 1983 *Phys. Rev. Lett.* **51** 2310
Mason M G 1983 *Phys. Rev.* B **27** 748
Qiu S L, Pan X, Strongin M and Citrin P H 1987 *Phys. Rev.* B **36** 1292
Roy H-V, Fayet P, Patthey F, Schneider W-D, Delley B and Massobrio C 1994 *Phys. Rev.* B **49** 5611
[2] Hövel H, Grimm B, Pollmann M and Reihl B 1998 *Phys. Rev. Lett.* **81** 4608
[3] Busolt U, Cottancin E, Röhr H, Socaciu L, Leisner T and Wöste L 1999 *Appl. Phys.* B **68** 453
[4] Lehmann J, Merschdorf M, Pfeiffer W, Thon A, Voll S and Gerber G 2000 *Phys. Rev. Lett.* **85** 2921
[5] Hövel H 2001 *Appl. Phys.* A **72** 295
[6] Meiwes-Broer K-H (ed) 2000 *Metal Clusters at Surfaces* (Berlin: Springer) pp 151–74
[7] Cinchetti M, Oelsner A, Fecher G H, Elmers H J and Schönhense G 2003 *Appl. Phys. Lett.* **83** 1503
[8] Merschdorf M, Kennerknecht C, Willig K and Pfeiffer W 2002 *New J. Phys.* **4** 95
[9] Swiech W, Fecher G H, Ziethen Ch, Schmidt O, Schönhense G, Grzelakowski K, Schneider C M, Frömter R, Oepen H P and Kirschner J 1997 *J. Electron Spectrosc. Relat. Phenom.* **84** 171
[10] Nepijko S A, Sedov N N, Schmidt O, Schönhense G, Bao X and Huang W 2001 *J. Microsc.* **202** 480
[11] Schneider C M and Schönhense G 2002 *Rep. Prog. Phys.* **65** R1785
[12] Fauster Th and Steinmann W 1995 *Photonic Probes of Surfaces* ed Halevi P (*Electromagnetic Waves: Recent Developments in Research* vol 2) (Amsterdam: North-Holland) pp 347–411
[13] Hövel H, Becker Th, Bettac A, Reihl B, Tschudy M and Williams E J 1997 *J. Appl. Phys.* **81** 154
[14] Hahn J R and Kang H 2000 *Surf. Sci. Lett.* **446** L77

[15] Merschdorf M, Pfeiffer W, Thon A, Voll S and Gerber G 2000 *Appl. Phys.* A **71** 547
[16] For an overview on plasmon excitations in clusters we refer to the textbook Kreibig U and Vollmer M 1995 *Optical Properties of Metal Clusters* (Berlin: Springer)
[17] Tiggesbäumer J, Köller L, Meiwes-Broer K H and Liebsch A 1993 *Phys. Rev.* A **48** R17490
[18] Nilius N, Ernst N and Freund H-J 2000 *Phys. Rev. Lett.* **84** 3994
[19] Hövel H, Fritz S, Hilger A, Kreibig U and Vollmer M 1993 *Phys. Rev.* B **48** 18178
[20] Aeschlimann M, Schmuttenmaer C A, Elsayed-Ali H E, Miller R J D, Cao J, Gao Y and Mantell D A 1995 *J. Chem. Phys.* **102** 8606
[21] Fecher G H, Schmidt O, Hwu Y and Schönhense G 2002 *J. Electron Spectrosc. Relat. Phenom.* **126** 77
[22] Wolf M, Hotzel A, Knoesel E and Velic D 1999 *Phys. Rev.* B **59** 5926
[23] Lehmann J, Merschdorf M, Pfeiffer W, Thon A, Voll S and Gerber G 2000 *J. Chem. Phys.* **112** 5428
[24] Stuart H R and Hall D G 1998 *Phys. Rev. Lett.* **80** 5663
Stockmann M I, Faleev S V and Bergman D J 2002 *Phys. Rev. Lett.* **88** 067402